Supplementary Information

Aqueous photooxidation of live bacteria with hydroxyl radicals under clouds-like conditions: Insights into the production and transformation of biological and organic matter originating from bioaerosols

Yushuo Liu,[1,2] Patrick K. H. Lee,[1,3] Theodora Nah[1,2,3*]

[1]*School of Energy and Environment, City University of Hong Kong, Hong Kong SAR, China*
[2]*City University of Hong Kong Shenzhen Research Institute, Nanshan District, Shenzhen, China*
[3]*State Key Laboratory of Marine Pollution, City University of Hong Kong, Hong Kong SAR, China*

** To whom correspondence should be addressed: Theodora Nah (Email: theodora.nah@cityu.edu.hk, Tel: +852 3442 5578)*

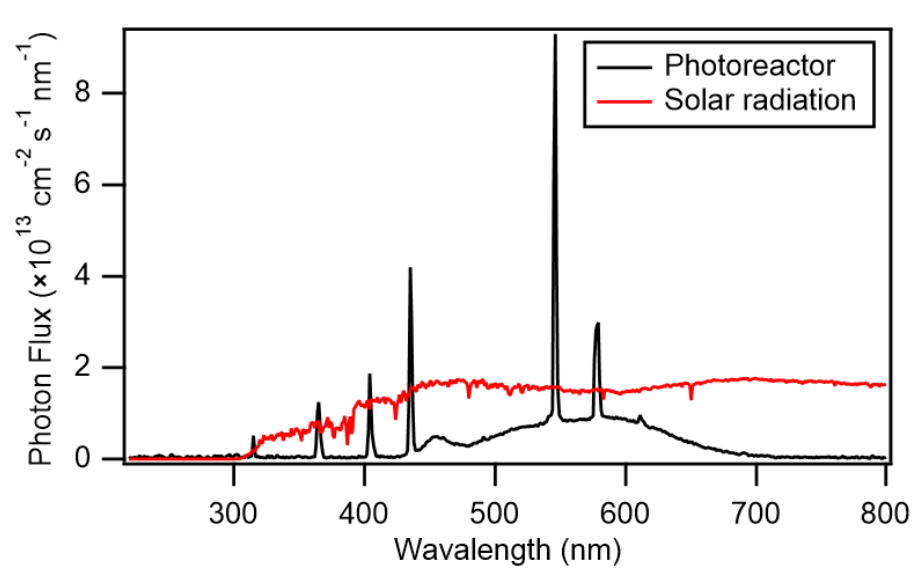

Figure S1. Photon flux inside of the photoreactor (black) and actinic flux for a fall day in Hong Kong in the morning (red).

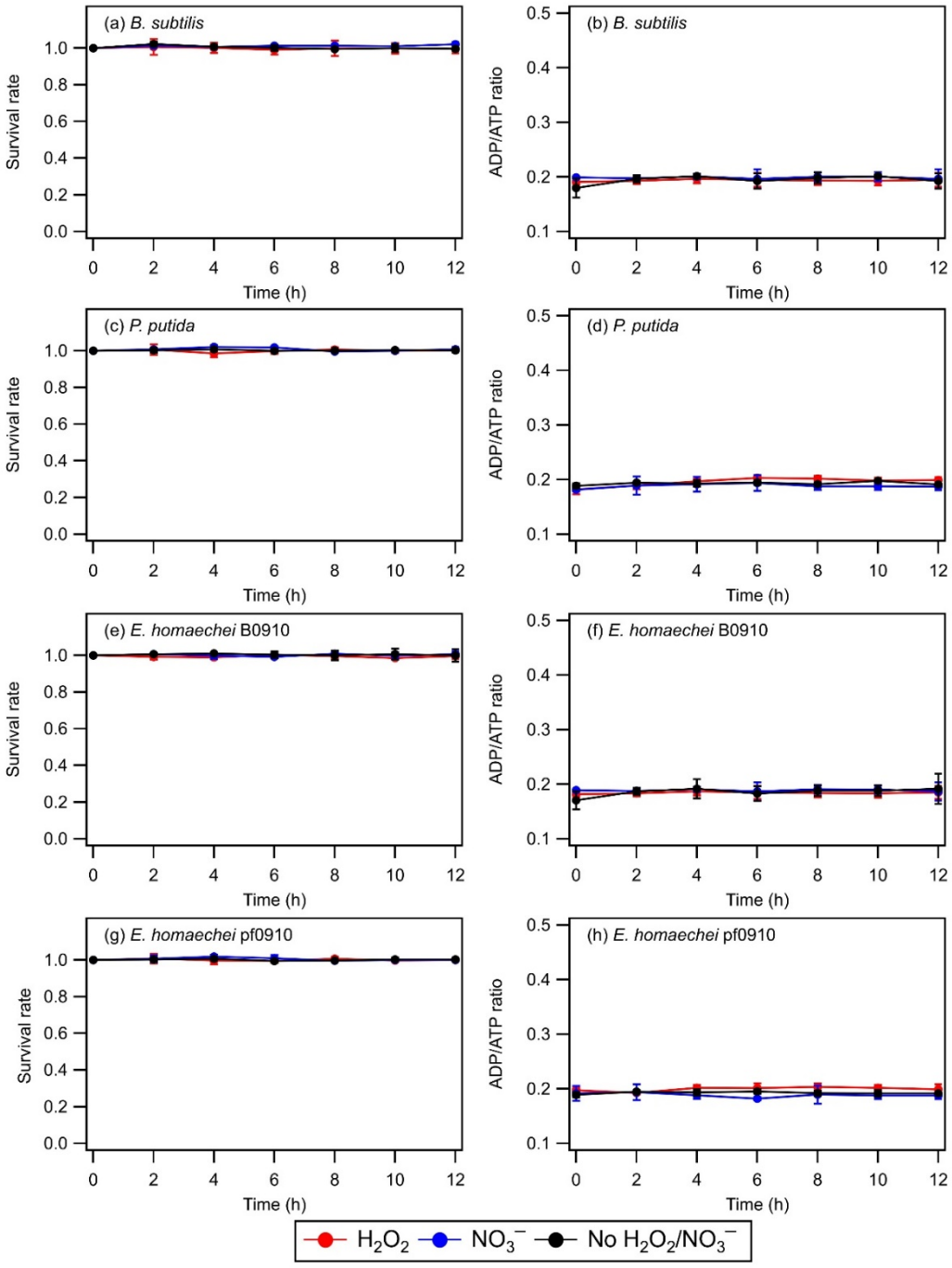

Figure S2. Survival rates and ADP/ATP ratios of the four bacteria strains in artificial cloud water in the absence and presence of H_2O_2 or NO_3^- at pH 5.2 under dark conditions over time. The survival rate is defined as the number concentration of culturable viable cells divided by the initial number concentration of culturable viable cells at time point 0 min. Error bars represent one standard deviation from the mean of biological triplicates.

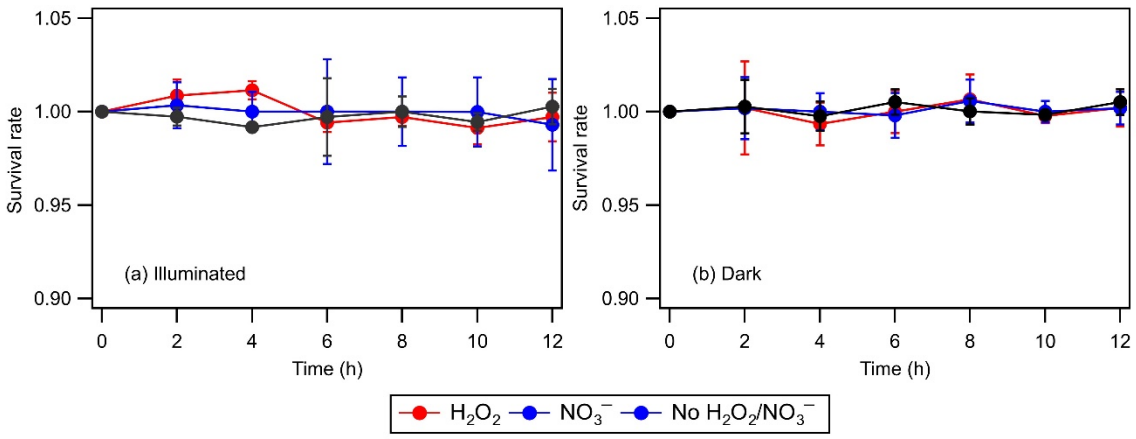

Figure S3. Survival rates of *B. subtilis* endospores in artificial cloud water in the absence and presence of H_2O_2 or NO_3^- at pH 5.2 under (a) illuminated and (b) dark conditions over time. The survival rate is defined as the number concentration of culturable viable cells divided by the initial number concentration of culturable viable cells at time point 0 min. Error bars represent one standard deviation from the mean of biological triplicates.

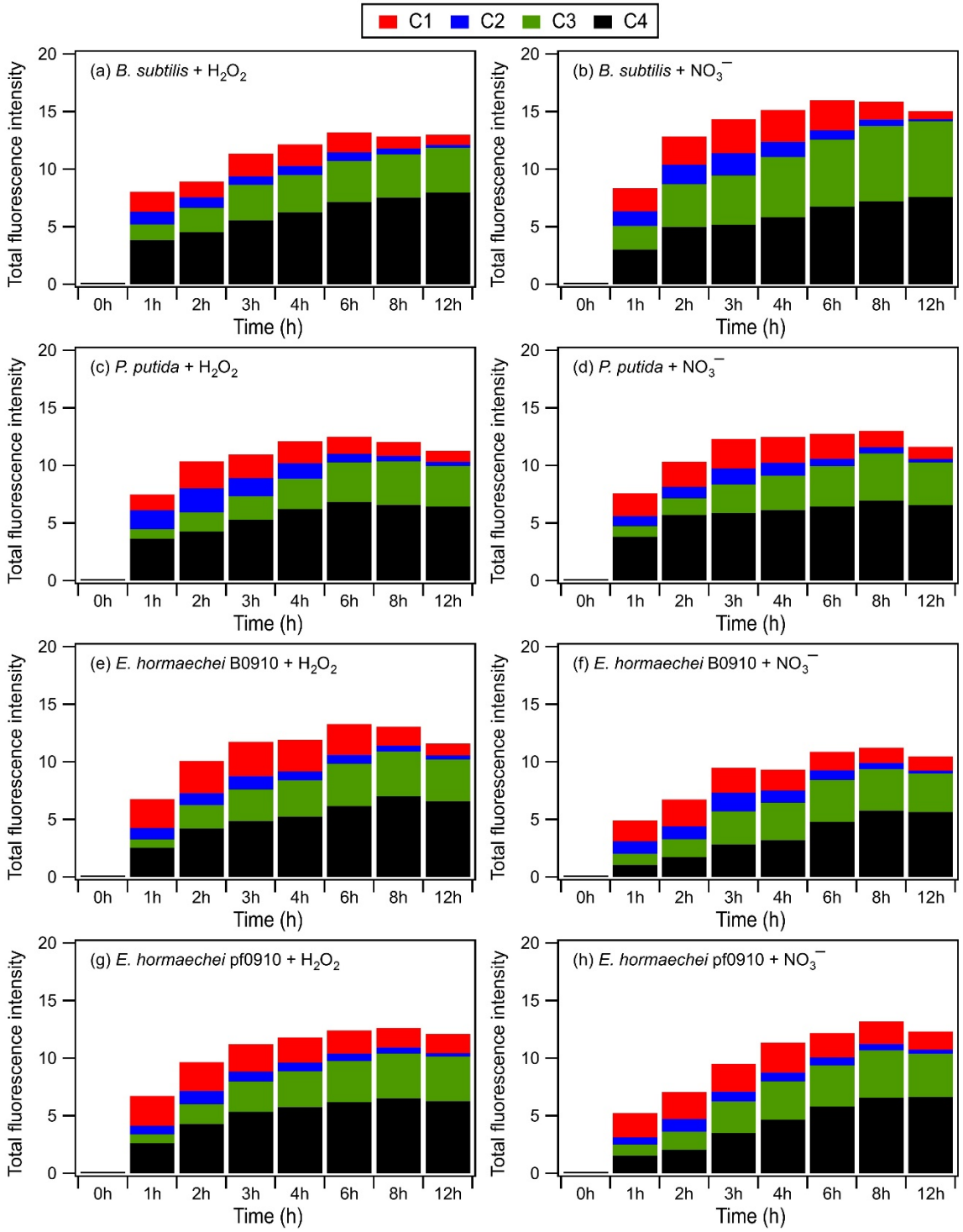

Figure S4. Time evolution of EEM fluorescent components 1, 2, 3, and 4 during photooxidation initiated by the photolysis of (a, c, e, and g) H_2O_2, and (b, d, f, and h) NO_3^-. These four components were extracted from PARAFAC analyses. Components 1, 2, 3, and 4 were assigned as tryptophan-like, tyrosine-like, HULIS-1, and HULIS-2 chromophores, respectively.

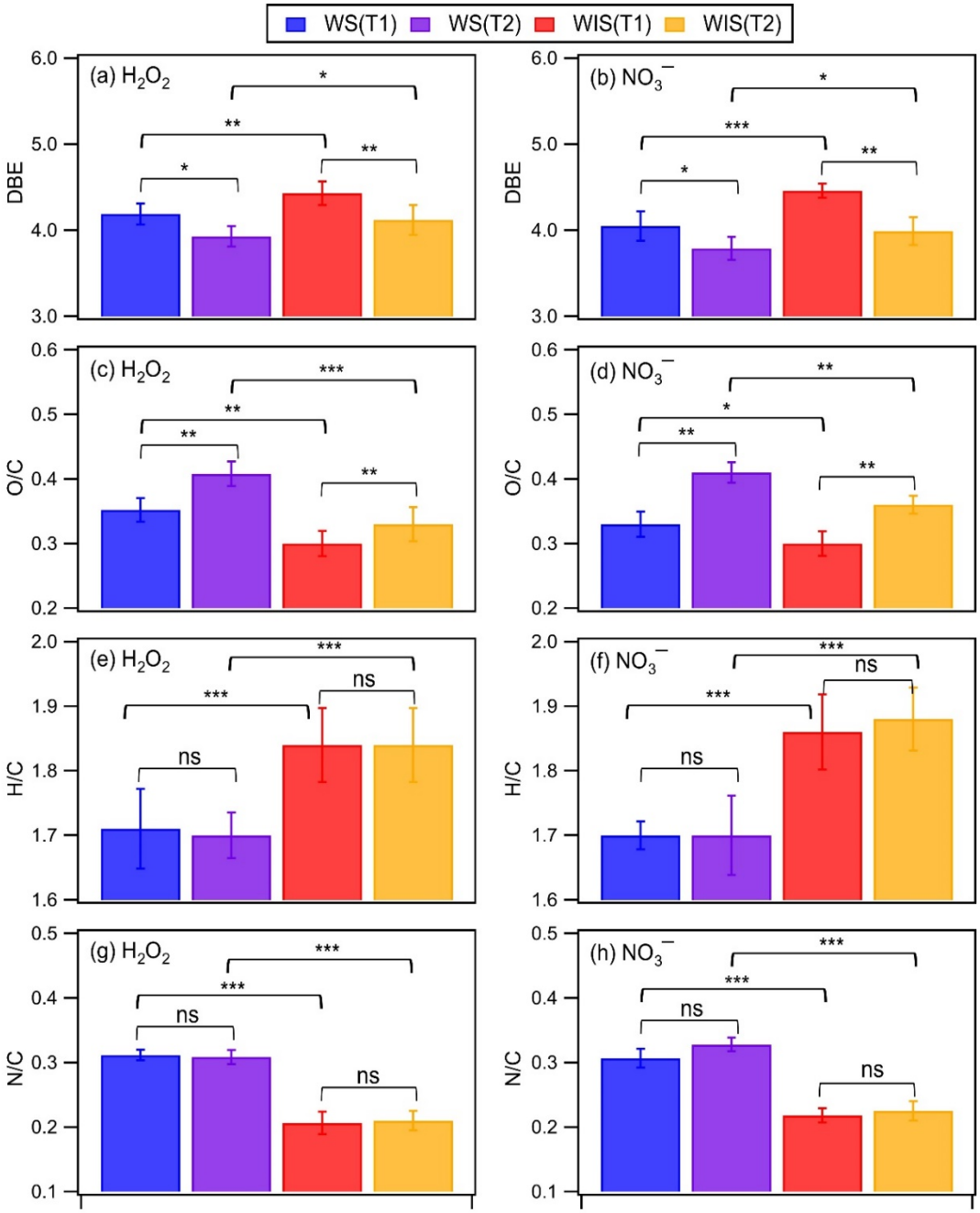

Figure S5. Profiles of intensity-weighted average values for WS and WIS samples obtained during the photooxidation of *B. subtilis* initiated by H_2O_2 and NO_3^- photolysis at time points T1 and T2: (a) and (b) DBE; (c) and (d) O/C; (e) and (f) H/C; (g) and (h) N/C. Time point T1 is when the survival rate of the bacterial strain first reaches zero, and time point T2 is 6 hours after T1. Error bars represent one standard deviation from the mean of triplicate measurements. Statistical analysis was performed using the Student's t-test (ns: not significant, *: $p < 0.05$, **: $p < 0.01$, ***: $p < 0.001$).

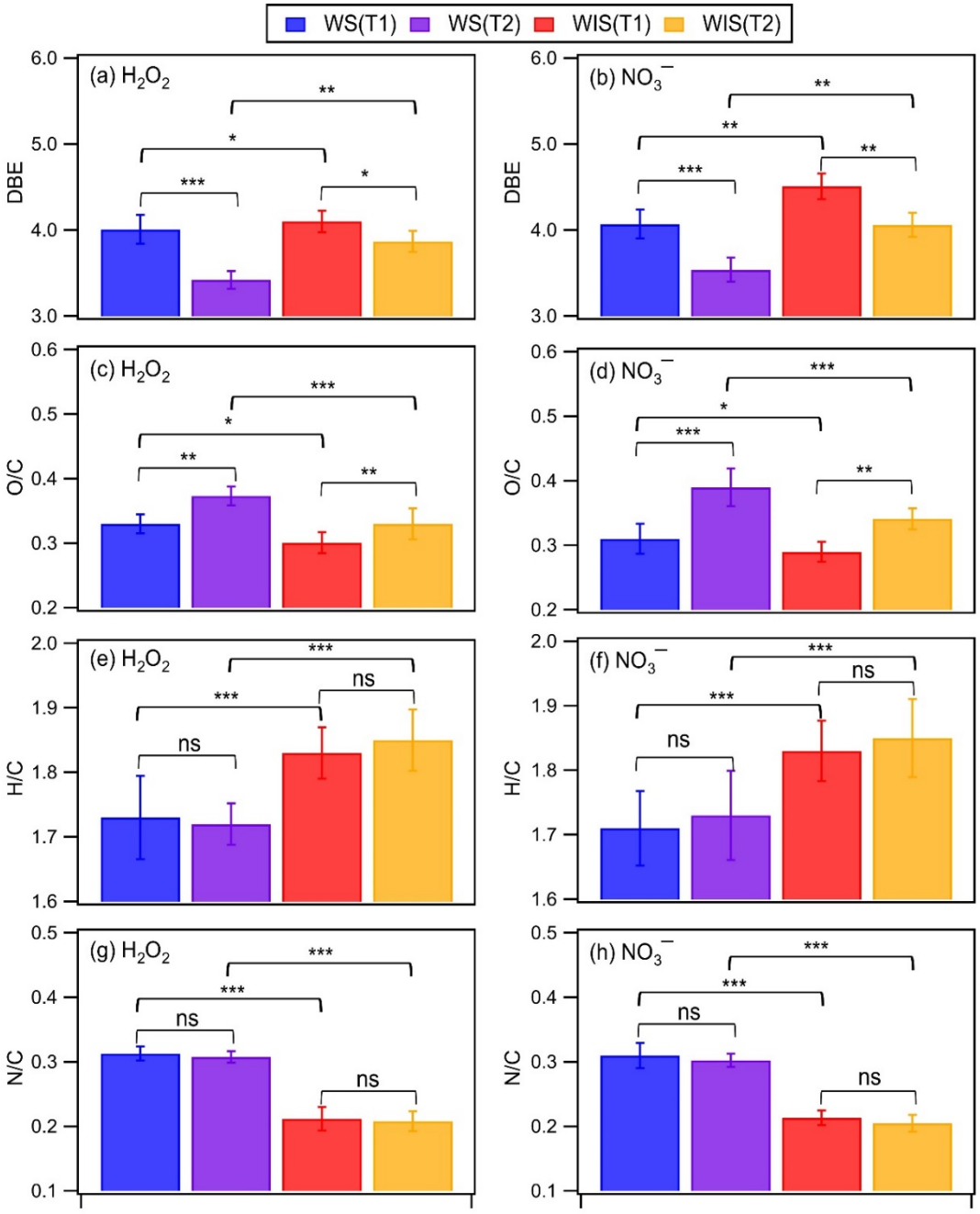

Figure S6. Profiles of intensity-weighted average values for WS and WIS samples obtained during the photooxidation of *P. putida* initiated by H_2O_2 and NO_3^- photolysis at time points T1 and T2: (a) and (b) DBE; (c) and (d) O/C; (e) and (f) H/C; (g) and (h) N/C. Time point T1 is when the survival rate of the bacterial strain first reaches zero, and time point T2 is 6 hours after T1. Error bars represent one standard deviation from the mean of triplicate measurements. Statistical analysis was performed using the Student's t-test (ns: not significant, *: $p < 0.05$, **: $p < 0.01$, ***: $p < 0.001$).

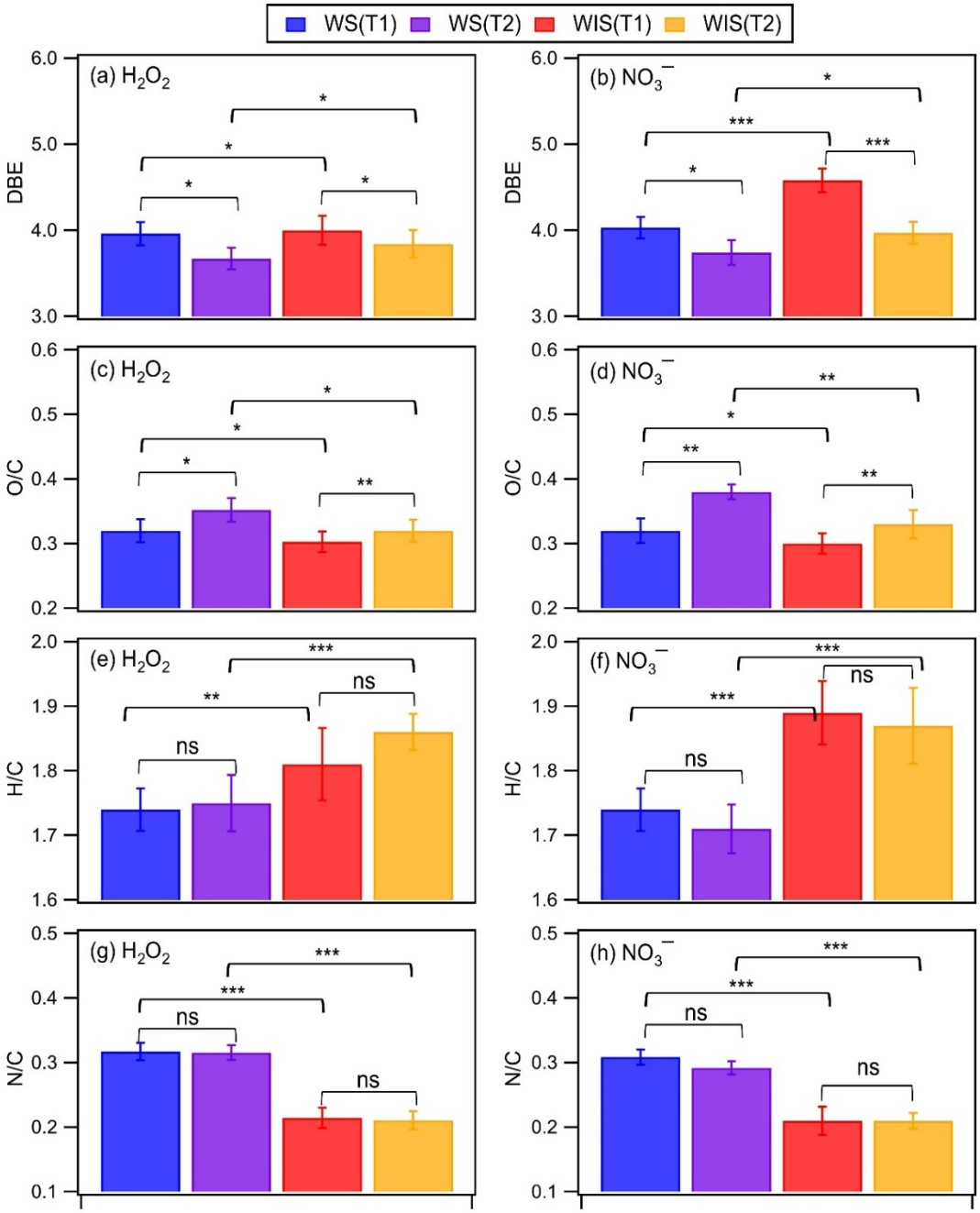

59

60 **Figure S7.** Profiles of intensity-weighted average values for WS and WIS samples obtained
61 during the photooxidation of *E. hormaechei* B0910 initiated by H_2O_2 and NO_3^- photolysis at
62 time points T1 and T2: (a) and (b) DBE; (c) and (d) O/C; (e) and (f) H/C; (g) and (h) N/C. Time
63 point T1 is when the survival rate of the bacterial strain first reaches zero, and time point T2 is
64 6 hours after T1. Error bars represent one standard deviation from the mean of triplicate
65 measurements. Statistical analysis was performed using the Student's t-test (ns: not significant,
66 *: $p < 0.05$, **: $p < 0.01$, ***: $p < 0.001$).

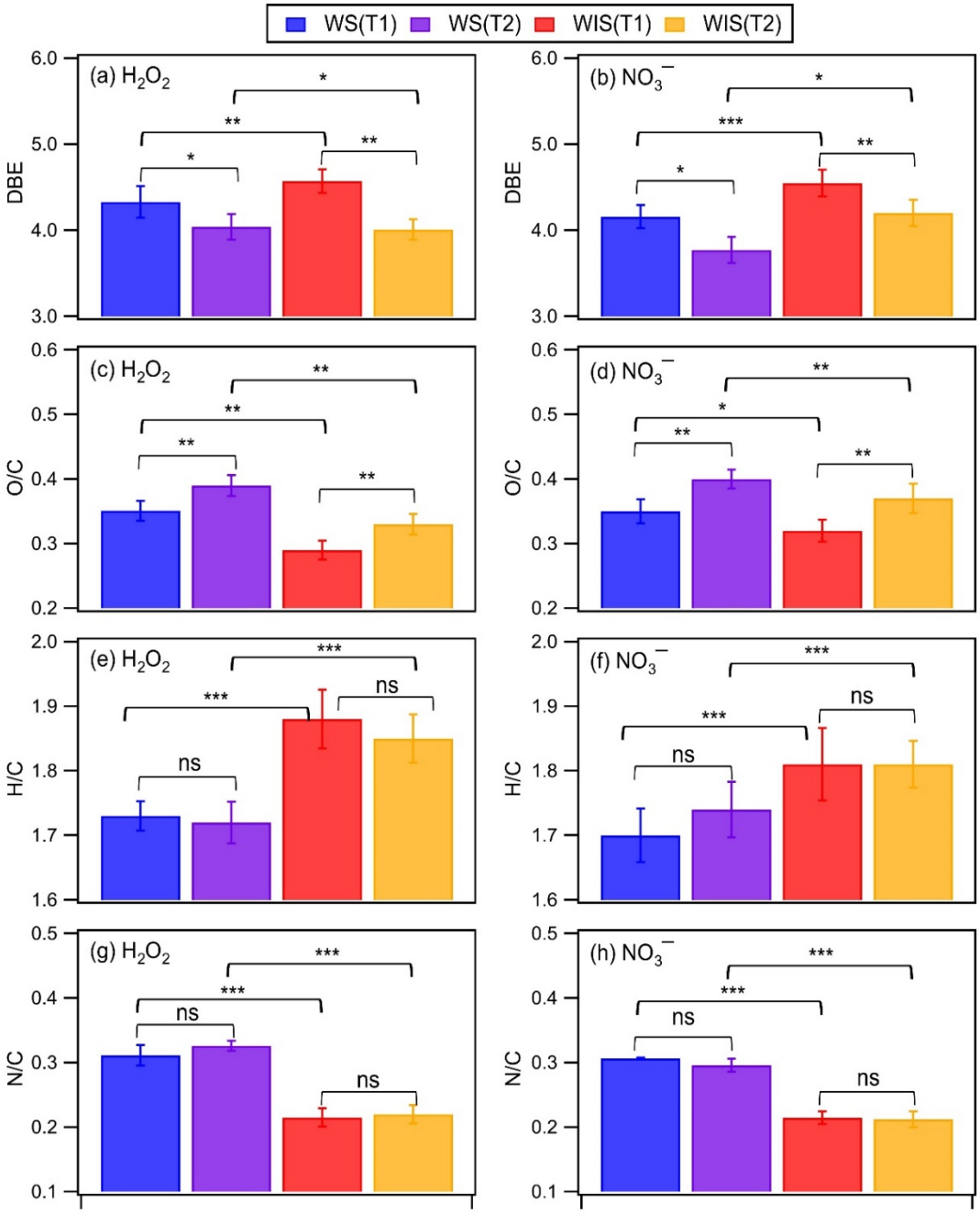

Figure S8. Profiles of intensity-weighted average values for WS and WIS samples obtained during the photooxidation of *E. hormaechei* pf0910 initiated by H_2O_2 and NO_3^- photolysis at time points T1 and T2: (a) and (b) DBE; (c) and (d) O/C; (e) and (f) H/C; (g) and (h) N/C. Time point T1 is when the survival rate of the bacterial strain first reaches zero, and time point T2 is 6 hours after T1. Error bars represent one standard deviation from the mean of triplicate measurements. Statistical analysis was performed using the Student's t-test (ns: not significant, *: $p < 0.05$, **: $p < 0.01$, ***: $p < 0.001$).

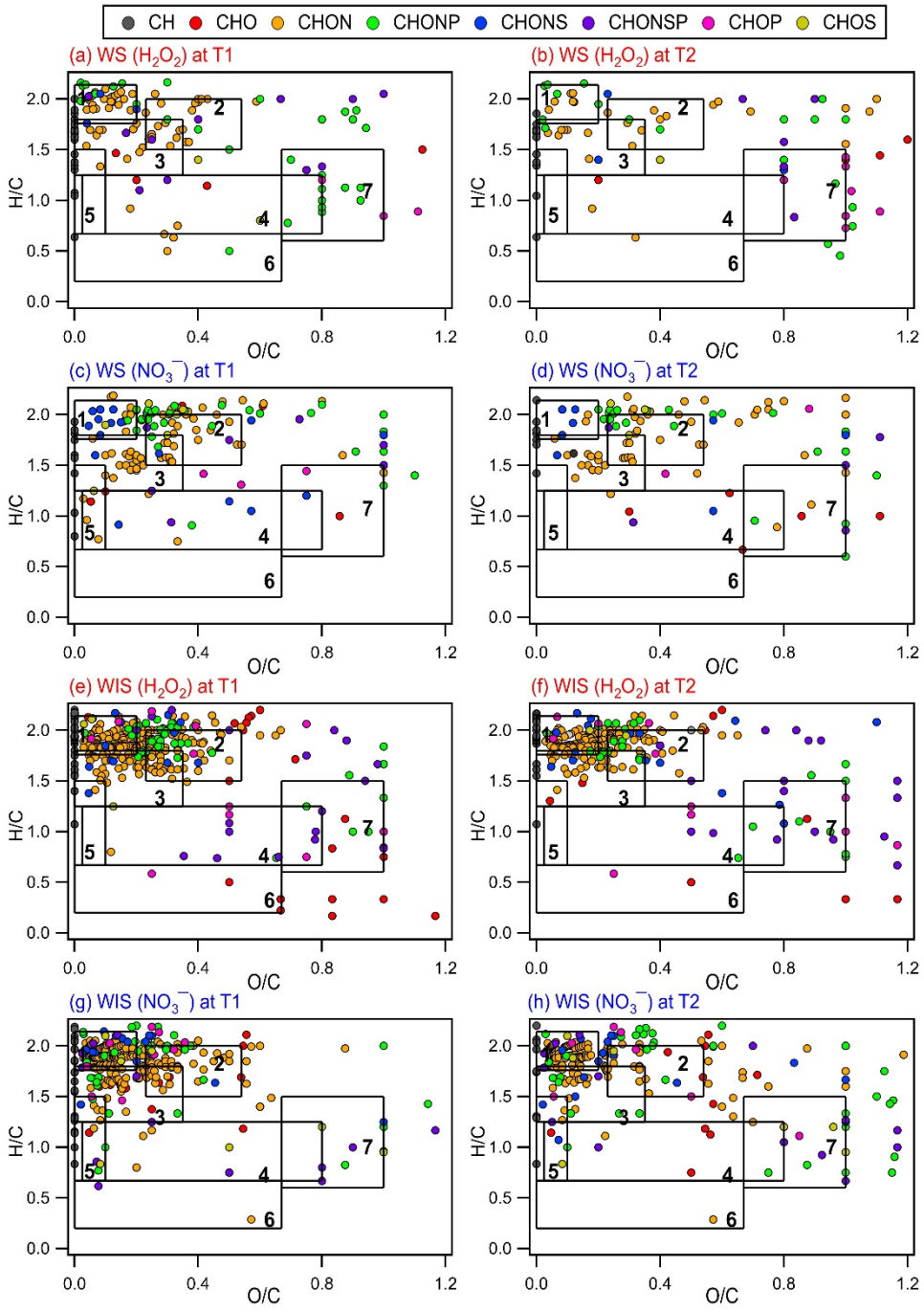

Figure S9. VK diagrams of WS and WIS compounds from *P. putida* at time points T1 and T2 during photooxidation initiated by the photolysis of (a, b, e, and f) H_2O_2, and (c, d, g, and h) NO_3^-. Time point T1 is when the survival rate of the bacterial strain first reaches zero, and time point T2 is 6 hours after T1. The VK diagrams are divided into seven chemical classes based on their combined O/C and H/C ratios: (1) lipids, (2) peptides, (3) terpenoids, (4) polyketides, (5) unsaturated hydrocarbons, (6) aromatic structures, (7) HOCs. The symbols are colored based on compositions (CH, CHO, CHON, CHONP, CHONS, CHONSP, CHOP, and CHOS).

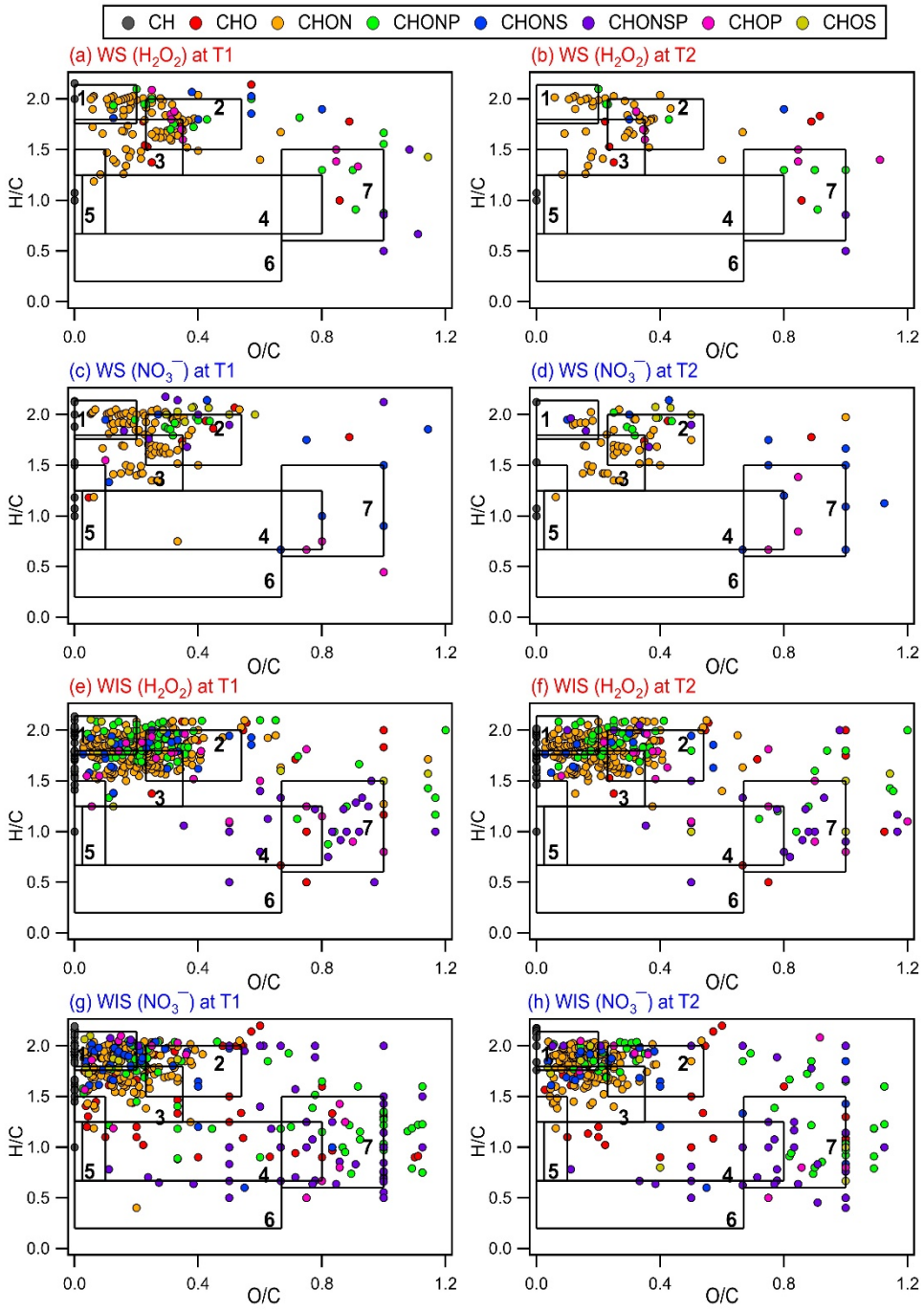

Figure S10. VK diagrams of WS and WIS compounds from *E. hormaechei* B0910 at time points T1 and T2 during photooxidation initiated by the photolysis of (a, b, e, and f) H_2O_2, and (c, d, g, and h) NO_3^-. Time point T1 is when the survival rate of the bacterial strain first reaches zero, and time point T2 is 6 hours after T1. The VK diagrams are divided into seven chemical classes based on their combined O/C and H/C ratios: (1) lipids, (2) peptides, (3) terpenoids, (4) polyketides, (5) unsaturated hydrocarbons, (6) aromatic structures, (7) HOCs. The symbols are colored based on compositions (CH, CHO, CHON, CHONP, CHONS, CHONSP, CHOP, and CHOS).

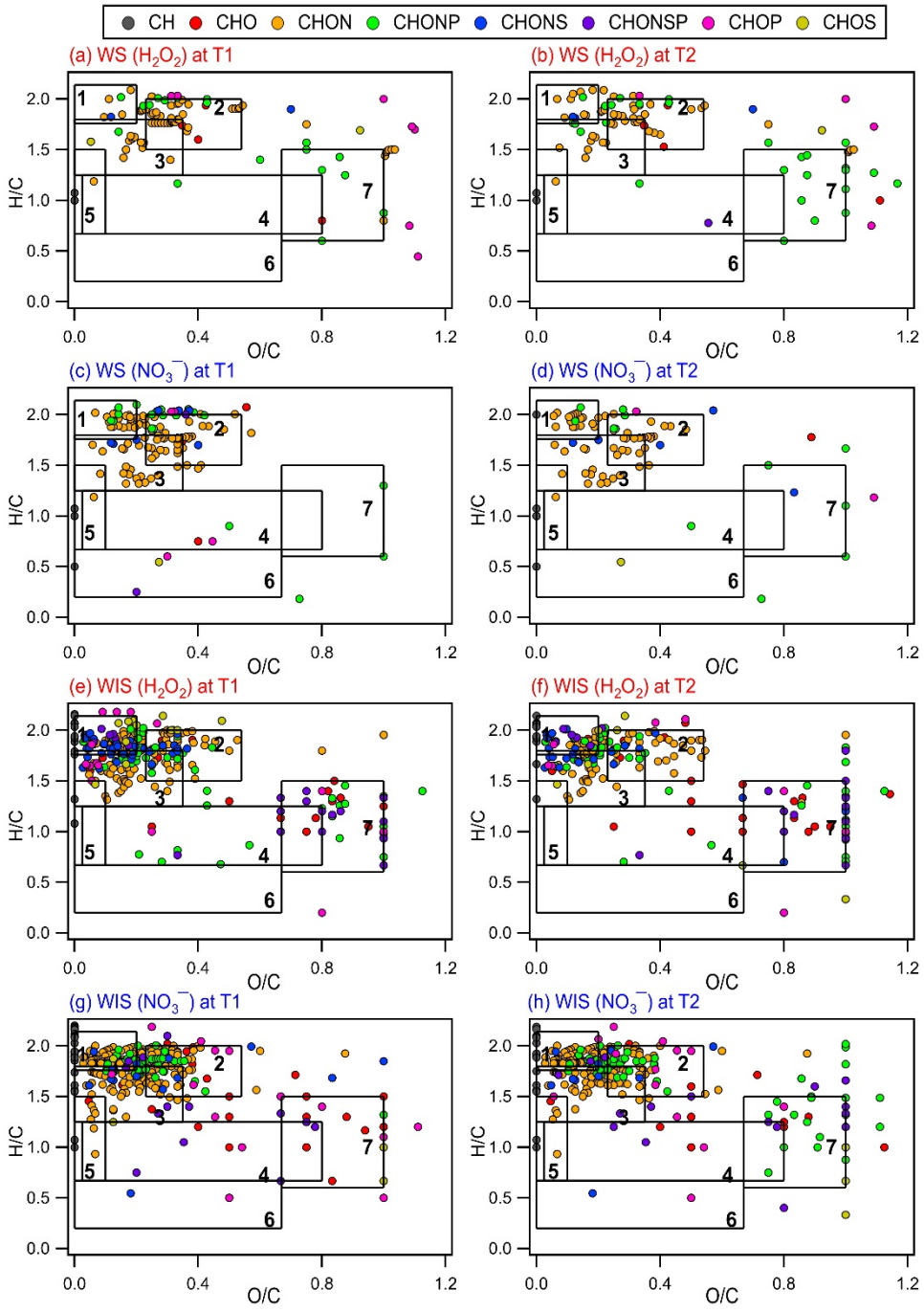

Figure S11. VK diagrams of WS and WIS compounds from *E. hormaechei* pf0910 at time points T1 and T2 during photooxidation initiated by the photolysis of (a, b, e, and f) H_2O_2, and (c, d, g, and h) NO_3^-. Time point T1 is when the survival rate of the bacterial strain first reaches zero, and time point T2 is 6 hours after T1. The VK diagrams are divided into seven chemical classes based on their combined O/C and H/C ratios: (1) lipids, (2) peptides, (3) terpenoids, (4) polyketides, (5) unsaturated hydrocarbons, (6) aromatic structures, (7) HOCs. The symbols are colored based on compositions (CH, CHO, CHON, CHONP, CHONS, CHONSP, CHOP, and CHOS).

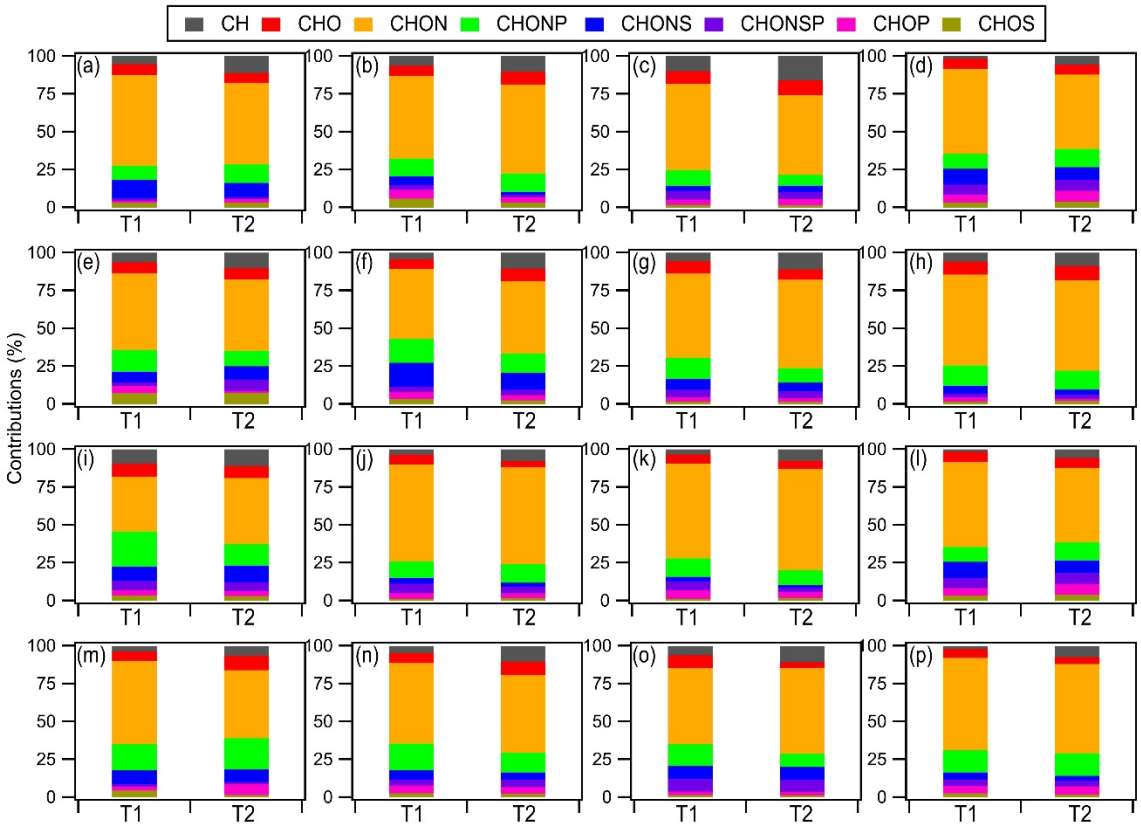

Figure S12. Contributions of the different classes of WS compounds from (a) *B. subtilis*, (b) *P. putida*, (c) *E. hormaechei* B0910, and (d) *E. hormaechei* pf0910 during photooxidation initiated by H_2O_2 photolysis; WS compounds from (e) *B. subtilis*, (f) *P. putida*, (g) *E. hormaechei* B0910, and (h) *E. hormaechei* pf0910 during photooxidation initiated by NO_3^- photolysis. Also shown are contributions of the different classes WIS compounds from (i) *B. subtilis*, (j) *P. putida*, (k) *E. hormaechei* B0910, and (l) *E. hormaechei* pf0910 during photooxidation initiated by H_2O_2 photolysis; WIS compounds from (m) *B.subtilis*, (n) *P.putida*, (o) *E. hormaechei* B0910, and (p) *E. hormaechei* pf0910 during photooxidation initiated by NO_3^- photolysis.

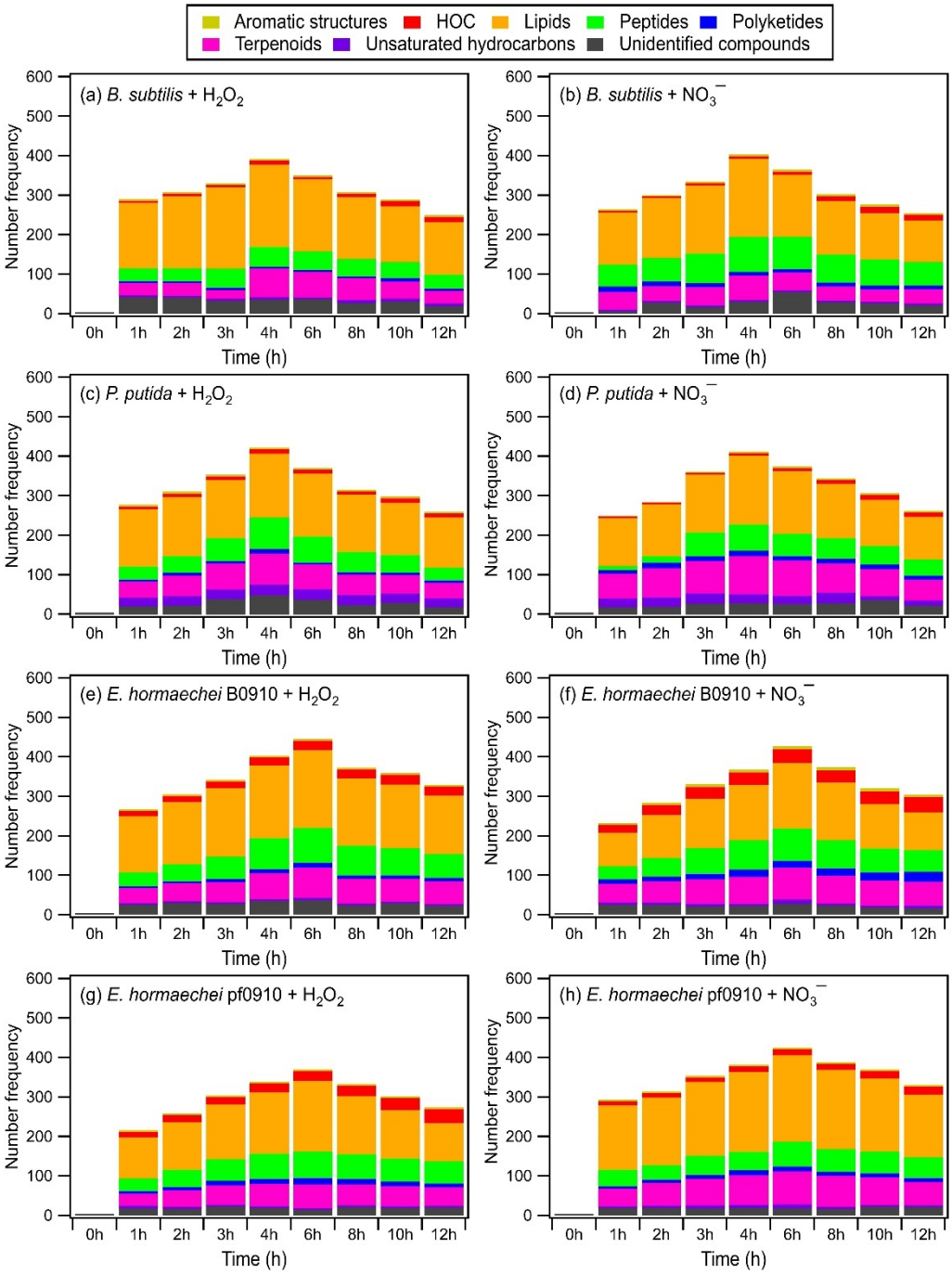

112

113 **Figure S13.** Time evolution of the number of WIS compounds from the four bacterial strains
114 detected by the UPLC-MS during photooxidation initiated by the photolysis of (a, c, e, and g)
115 H_2O_2, and (b, d, f, and h) NO_3^-.

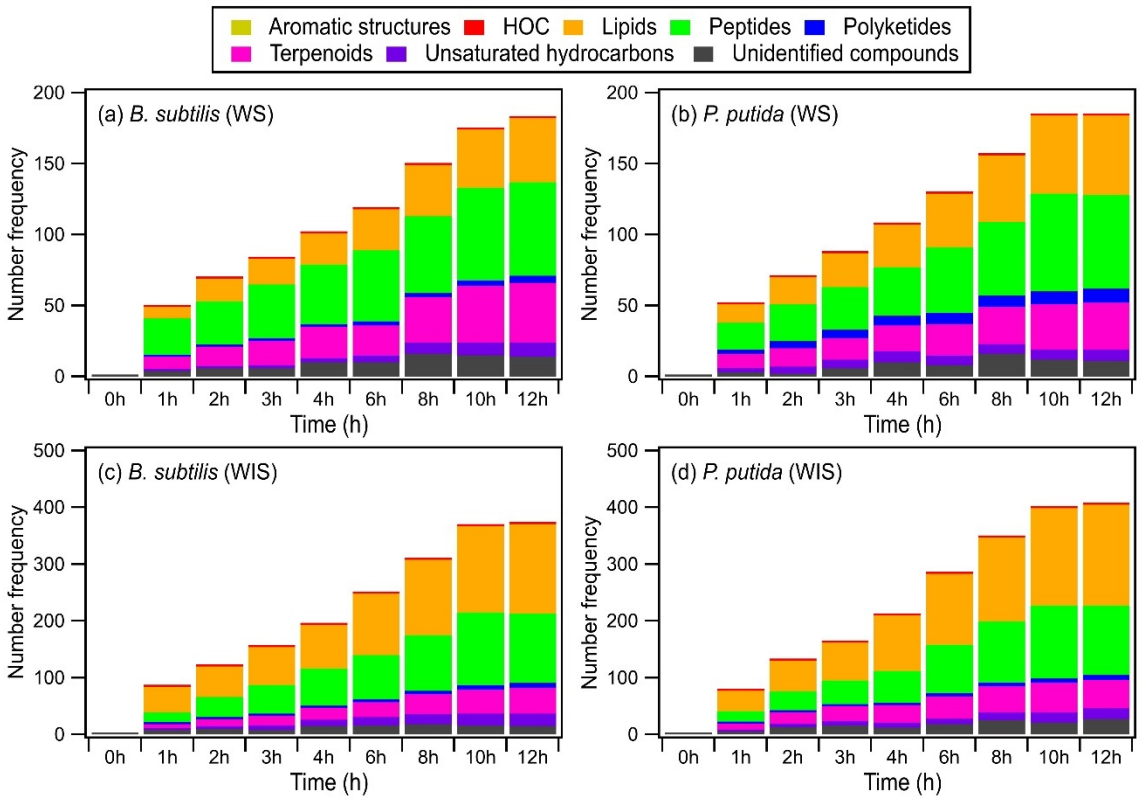

116

117 **Figure S14.** Time evolution of the number of WS and WIS compounds from *B. subtilis* and *P.*
118 *putida* detected by the UPLC-MS during illumination in the absence of H_2O_2 or NO_3^-.

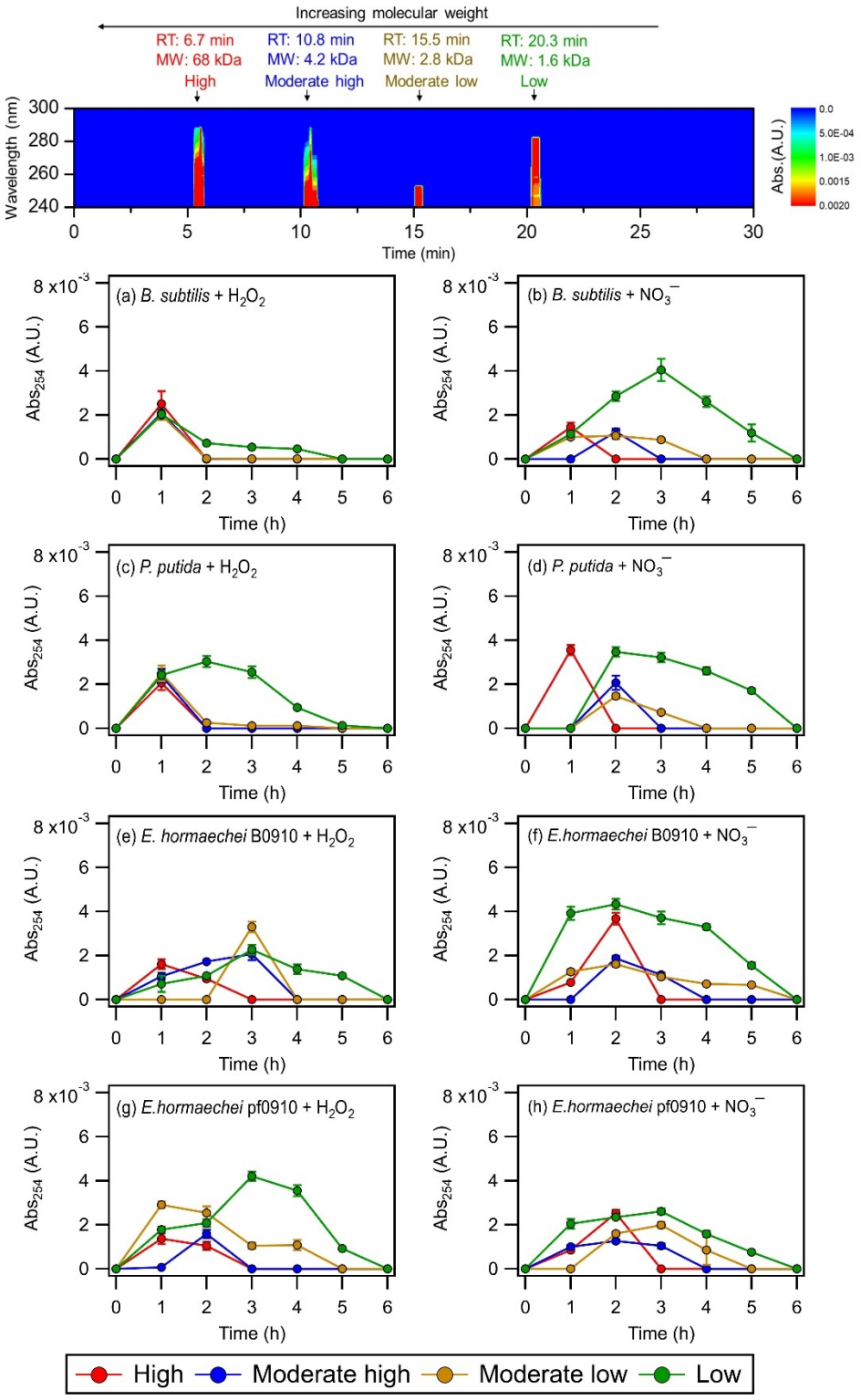

Figure S15. The top panel shows a typical SEC/UV-Visible absorption chromatogram of a WS extract from *B. subtilis* during photooxidation initiated by H_2O_2 photolysis. Based on the calibrations performed using sodium polystyrene sulfonate standards, the elution times 6.7 min, 10.8 min, 15.5 min, and 20.3 min corresponded to molecular weights of around 68 kDa, 4.2 kDa, 2.8 kDa, and 1.6 kDa, respectively. Similar SEC/UV-Visible absorption chromatograms

were obtained for the four bacterial strains during photooxidation initiated by H_2O_2 and NO_3^-. For simplicity, compounds that eluted between 5 to 10 min, between 10 to 15 min, between 15 to 20 min, and after 20 min were classified as high, moderate high, moderate low, and low molecular weight fractions, respectively. Also shown are the time series of the absorption at wavelength 254 nm for high, moderate high, moderate low, and low molecular weight fractions from (a and b) *B. subtilis*, (c and d) *P. putida*, (e and f) *E. hormaechei* B0910, and (g and h) *E. hormaechei* pf0910 during photooxidation initiated by H_2O_2 or NO_3^- photolysis.

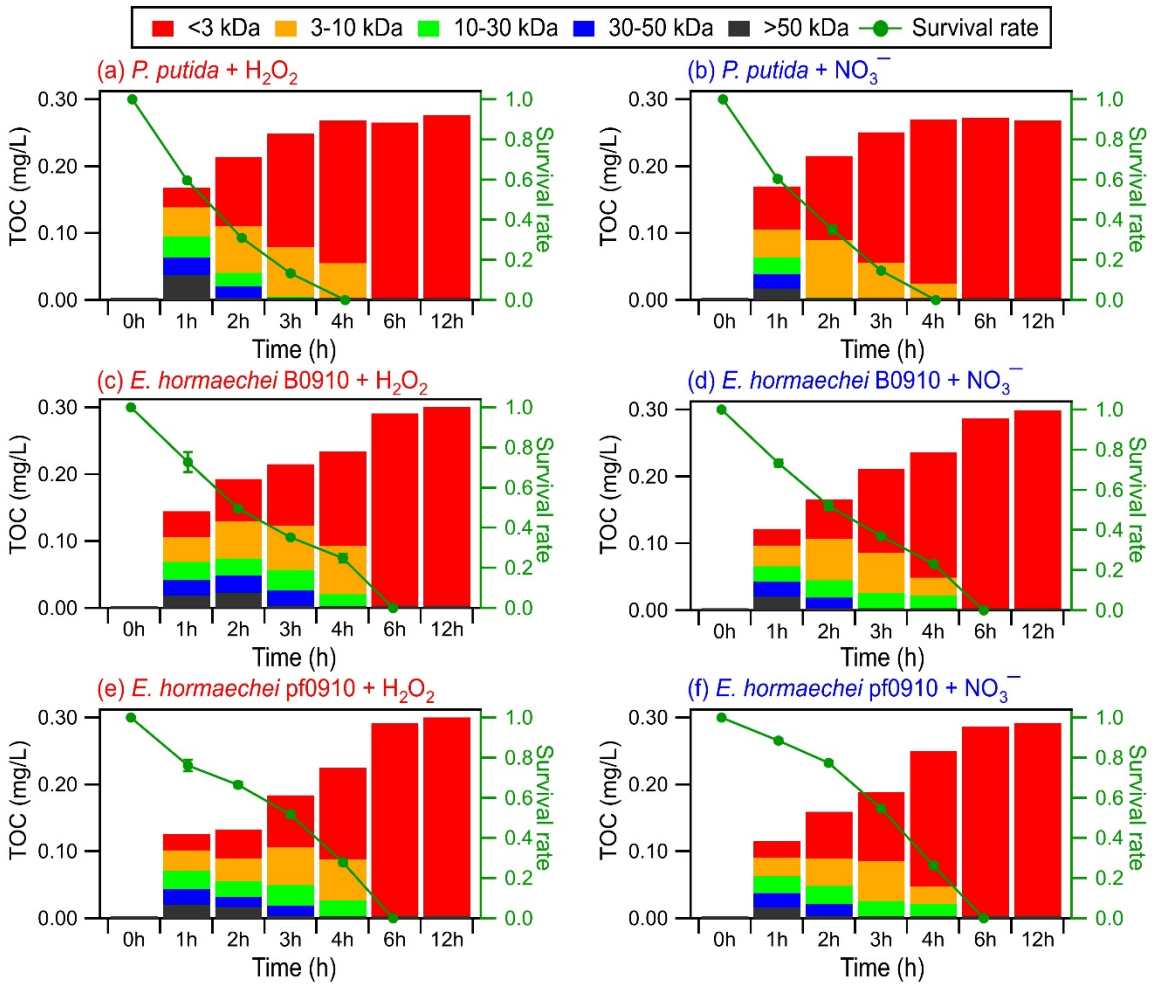

Figure S16. TOC concentrations of different molecular weight-fractionated (<3 kDa, 3 to 10 kDa, 10 to 30 kDa, 30 to 50 kDa, and >50 kDa) filtrates from (a and b) *P. putida*, (c and d) *E. hormaechei* B0910, and (e and f) *E. hormaechei* pf0910 during photooxidation initiated by H_2O_2 and NO_3^- photolysis.

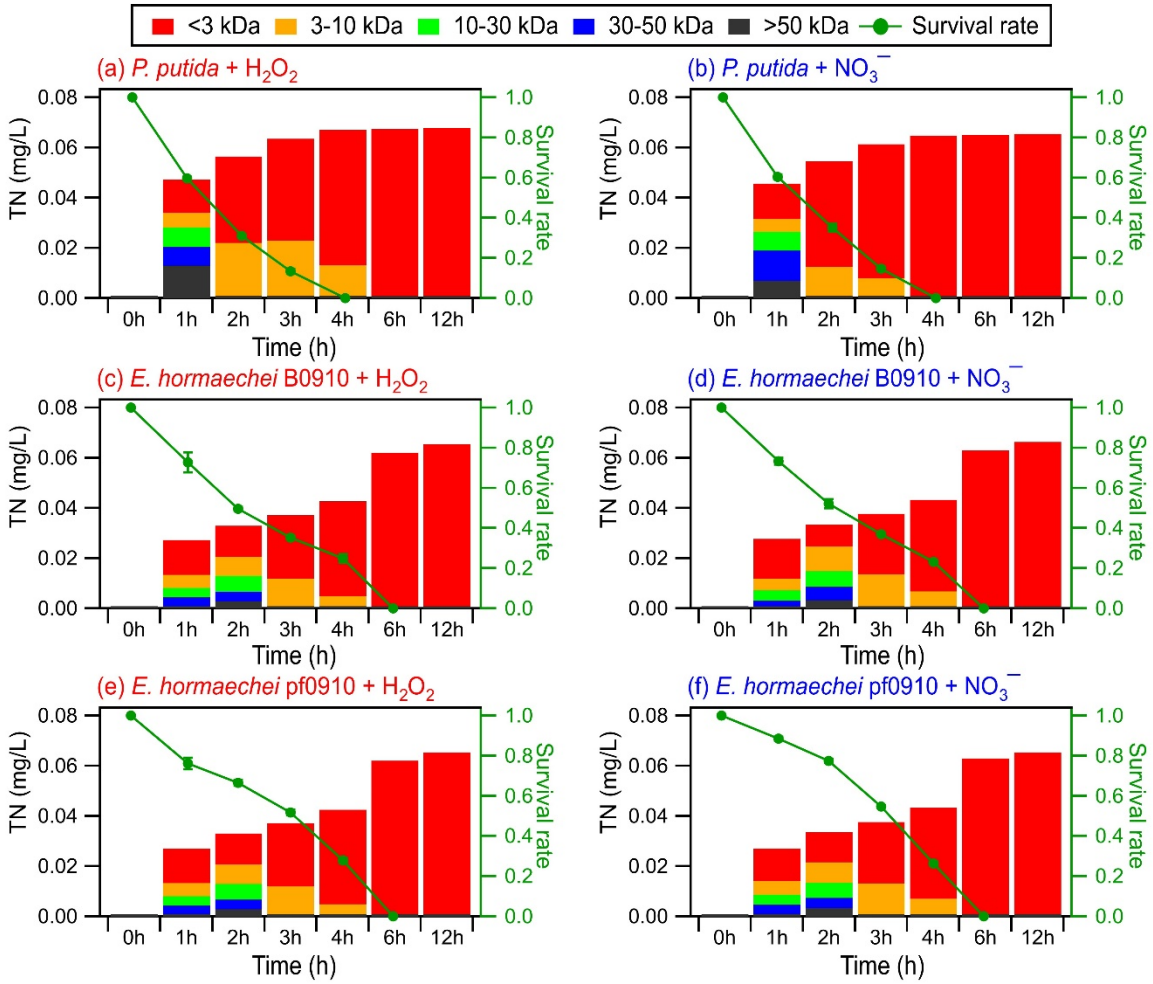

137

138 **Figure S17.** TN concentrations of different molecular weight-fractionated (<3 kDa, 3 to 10
139 kDa, 10 to 30 kDa, 30 to 50 kDa, and >50 kDa) filtrates from (a and b) *P. putida*, (c and d) *E.*
140 *hormaechei* B0910, and (e and f) *E. hormaechei* pf0910 during photooxidation initiated by
141 H_2O_2 and NO_3^- photolysis.

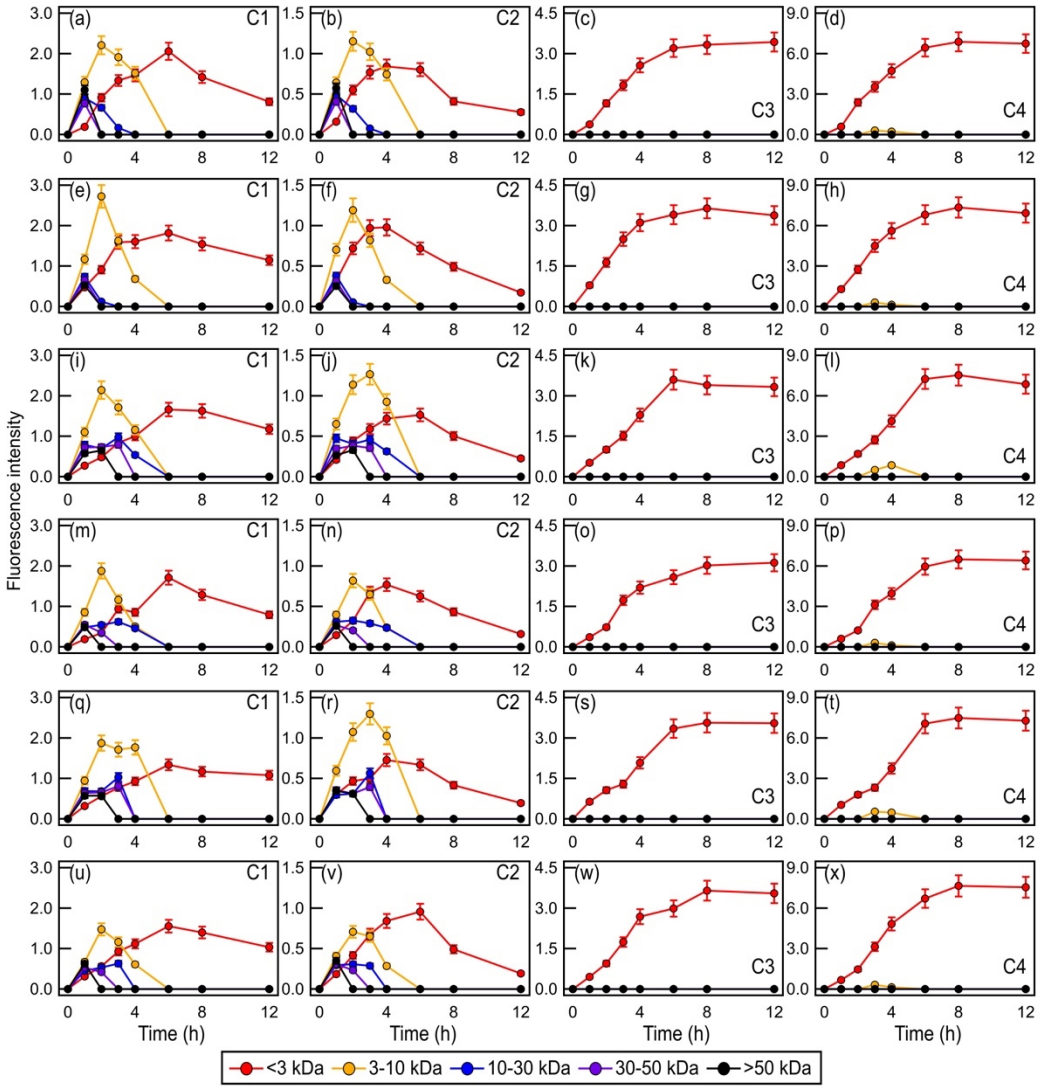

142

143 **Figure S18.** Time evolution of the four PARAFAC-extracted components in the five molecular
144 weight-fractionated filtrates from (a to d) *P. putida*, (i to l) *E. hormaechei* B0910, and (q to t)
145 *E. hormaechei* pf0910 during photooxidation initiated by H_2O_2 photolysis. Also shown are the
146 time evolution of the four PARAFAC-extracted components in the five molecular weight-
147 fractionated filtrates from (e to h) *P. putida*, (m to p) *E. hormaechei* B0910, and (u to x) *E.*
148 *hormaechei* pf0910 during photooxidation initiated by NO_3^- photolysis. Components C1, C2,
149 C3, and C4 were assigned as tryptophan-like, tyrosine-like, HULIS-1, and HULIS-2
150 chromophores, respectively.

151

152

153

Table S1. Chemical composition of the artificial cloud water used to prepare bacteria cells and perform experiments. Also shown are their mean concentrations in cloud water at Tai Mo Shan reported by Li et al. (2020).[1]

Organic ion	Artificial cloud water medium (μM)	Mean concentration at Tai Mo Shan (μM)	Inorganic ion	Artificial cloud water medium (μM)	Mean concentration at Tai Mo Shan (μM)
Formate	17.1	17.1	Na^+	250[a]	93
Acetate	10.2	10.2	NH_4^+	200	235
Pyruvate	2.7	2.7	K^+	10	8
Oxalate	10.3	10.3	Mg^{2+}	23	23
			Ca^{2+}	49	49
			Cl^-	138	138
			SO_4^{2-}	200[b]	305

[a] While the Na^+ concentration in the artificial cloud water medium is higher than its average concentration in cloud water at Tai Mo Shan, it still falls within the concentration range measured in cloud water at Tai Mo Shan (4 to 447 μM). The higher Na^+ concentration in the artificial cloud water was due to the addition of NaOH to achieve pH 5.2. The Na^+ concentration was maintained at 250 μM in experiments where $NaNO_3$ was used as the ·OH photochemical precursor.

[b] While the SO_4^{2-} concentration in the artificial cloud water medium is lower than its average concentration in cloud water at Tai Mo Shan, it still falls within the concentration range measured in cloud water at Tai Mo Shan (3 to 1340 μM). A lower SO_4^{2-} concentration was used in the artificial cloud water to achieve pH 5.2.

Table S2. Identified components from EEM fluorescence spectra by PARAFAC analysis

Component	Excitation (nm) /Emission (nm)	Putative chromophores
C1	270-280/330-340	Tryptophan-like
C2	275/305	Tyrosine-like
C3	250/460-520	HULIS-1
C4	240/392	HULIS-2

Table S3. Stoichiometric ranges of the seven chemical classes in the Van Krevelen diagrams.

Chemical class	H/C	O/C
Lipids[2]	$1.76 \leq H/C \leq 2.14$	$0.00 \leq O/C \leq 0.30$
Peptides[3]	$1.50 \leq H/C \leq 2.00$	$0.23 \leq O/C \leq 0.54$
Terpenoids[2]	$1.25 \leq H/C \leq 1.80$	$0.00 \leq O/C \leq 0.35$
Polyketides[2]	$0.67 \leq H/C \leq 1.25$	$0.02 \leq O/C \leq 0.80$
Unsaturated hydrocarbons[3]	$0.67 \leq H/C \leq 1.50$	$0.00 \leq O/C \leq 0.10$
Aromatic structures[3]	$0.20 \leq H/C \leq 0.67$	$0.00 \leq O/C \leq 0.67$
Highly oxygenated compounds[4]	$0.60 \leq H/C \leq 1.50$	$0.67 \leq O/C \leq 1.00$

Section S1. Preparation of *Bacillus subtilis* endospore suspension

Nutrient agar supplemented with 50 mg/L manganese sulfate (NAMS agar) was used as the sporulation medium.[5] The 200 μL of serial diluted *Bacillus subtilis* vegetative cells was deposited on the NAMS agar and incubated for 72 h at 30 ℃. Endospores were harvested by depositing 5 mL of sterile distilled water on the surface of each plate and gently rubbing it with a sterile bent glass rod. The suspensions of cells and spores were centrifuged for 10 min at 4000 xg at 10 °C. The supernatant fluid was then discarded. This procedure was repeated twice. The final pellet was suspended in sterile distilled cold water (5 °C). Endospore suspensions were stored at 4 °C prior to use in experiments. Before their use in experiments, the refrigerated endospore suspension was first brought up to room temperature. 1 mL of the endospore suspension was next deposited into 5 mL of sterile distilled water at 80 °C, which was then heated for 5 min to kill the vegetative cells. The endospores were subsequently re-suspended in artificial cloud water to an initial concentration of ~10^5 cells mL^{-1}. The number concentration of endospores in the suspension was determined by serial dilution and plating triplicate samples on nutrient agar. The plates were incubated at 30 °C for 24 h before counting commenced.

Section S2. Extraction of water-insoluble and water-soluble biological and organic compounds for UPLC-MS analysis

A modified Bligh & Dyer (BD) protocol was performed to extract water-insoluble organic compounds.[6] Briefly, 3 mL of methanol (Duskan, LC-MS grade)/chloroform (RCI, HPLC grade) (1:2, v/v) was added to a filtered 5 mL sample solution and vortexed for 5 min, after which the samples were centrifuged at 3000 rpm for 10 min at 10 ℃. The bottom layer was collected into a clean 2 mL centrifuge tube and dried in a concentrator using nitrogen gas. The dried extracts were redissolved in 500 μL of acetonitrile (Duskan, LC-MS grade) and stored at -20 ℃ prior to UPLC-MS analysis. Solid-phase extraction (SPE) was performed using hydrophobic lipophilic balanced (HLB) cartridges (Oasis HLB 6cc 500 mg, Waters, USA) to remove the inorganic salts and extract the water-soluble organic compounds. The HLB cartridges were first preconditioned with 1 mL methanol (Duskan, LC-MS grade) and 2 mL Milli-Q water. A 20 mL filtered sample solution was then loaded into the SPE cartridge and washed with 20 mL Milli-Q water under vacuum at a flow rate of 5 mL/min. The elution was performed by adding 1.5 mL methanol (Duskan, LC-MS grade). The eluent was then evaporated to dryness under nitrogen gas before being reconstituted in 500 μL methanol (Duskan, LC-MS grade).

Section S3. UPLC-MS parameters and the untargeted screening

The flow rate was fixed at 0.3 mL/min with ultra-pure water containing 5 mM ammonium acetate (Fisher, LC-MS grade) as mobile phase A and acetonitrile (Duskan, LC-MS grade) for mobile phase B. The following gradient program was used: 0 to 2 min 95 % A; 2 to 4 min linear gradient to 80 % B; 4 to 11 min linear gradient to 65 % B; 11 to 12.5 min 65 % B; 12.5 to 13 min linear gradient to 95 % B; 13 to 15 min equilibration wash with 95 % B. The information dependent analysis (IDA) acquisition was acquired with MS scan (100 to 1200 m/z) followed by MS/MS scan (50 to 1200 m/z) in positive ion mode and negative mode. The following MS conditions were used: 30 PSI curtain gas, 60 PSI ion source gas, 3000 V ESI ion spray voltage (-4000 V was used for negative mode), 320 ℃ source temperature, 10 V collision energy for MS, and 80 V declustering potential. MS/MS was acquired with a collision energy was 20 V with a 5 V spread.

Features were extracted by PatRoon[7] from the pretreated data by automatic identification of chromatographic peaks using the OpenMS function “FeatureFinderMetabo”. OpenMS is an open-source software library for LC-MS data management and analysis. The t settings for feature finding were a noise intensity threshold (“noise_threshold_int”) of 1000, a maximum chromatographic peak length (“max_trace_length”) of 240 s, and an allowed mass deviation of 5 ppm. A balance between quantity and quality was visually determined by applying settings that combined a high total number of features with a low number of features assigned to split peaks or noise. Equal features found across samples were grouped. Those “feature groups” were then filtered based on peak intensity (minimum 5000), ubiquitous presence in replicates, and a signal intensity of at least three times higher than sample blanks. The molecular formulas were calculated automatically for all feature groups. First, MS peak lists were generated from the feature groups using the “generateMSpeakLists” function from the patRoon R package. This function uses the mzR package to obtain MS and MS/MS spectra, and averages and filters the data. Candidate formulas were calculated with the “generateFormulas” function, which uses GenForm.[8] GenForm is an open-source package that generates molecular formulas by high-resolution MS and MS/MS data. It uses the accurate mass of the feature groups to calculate candidate formulas, and scores them based on matched theoretical/measured isotopic patterns. C, H, N, O, S, and P atoms were selected to be included in the formula calculations. Candidate formulas that did not meet basic chemical criteria were also excluded.[9, 10]

The double bond equivalent (DBE) value was calculated for each compound identified in the water insoluble and water soluble samples. The DBE value is equal to the total number of double bonds (C=C and C=O), and rings in a $C_cH_hO_oN_nS_sP_p$ molecule. The DBE values were calculated as follows:

$$DBE = 1 + \frac{1}{2}(2c - h + n + p) \quad (1)$$

O/C and H/C ratios were calculated from the compounds' molecular formulas. The average DBE values, O/C ratios, H/C ratios were calculated from all the assigned peaks in a given mass spectrum as follows:

$$DBE = \sum_i^{x_i DBE} \Big/ \sum_i x_i \quad (2)$$

$$O/C = \sum_i^{x_i o_i} \Big/ \sum_i x_i c_i \quad (3)$$

$$H/C = \sum_i^{x_i h_i} \Big/ \sum_i x_i c_i \quad (4)$$

$$N/C = \sum_i^{x_i n_i} \Big/ \sum_i x_i c_i \quad (5)$$

where x_i correspond to the measured ion intensities.

Section S4. EEM fluorescence measurements

The excitation and emission wavelength ranges were from 220 to 500 nm (5 nm step) and 200 to 600 nm (10 nm step), respectively. The fluorescence spectra were obtained in the "Signal/Reference" mode with instrumental bias correction. We followed the standard practices for EEM fluorescence spectra collection and processing. The inner filter effect was corrected by the absorbance spectrum measured with the UV–vis spectrophotometer.[11] The EEM fluorescence spectra of all the samples were corrected by subtracting the blank sample. First- and second-order Rayleigh scattering were removed by interpolation. Parallel factor analysis (PARAFAC) with non-negativity constraint was performed on the EEM spectra using

the R package stardom version 1.1.25.[12] Four components were identified based on comparisons of their extracted spectra to those reported in previous studies.[13-16] These four components were identified as Tryptophan-like, Tyrosine-like, HULIS-1, and HULIS-2 (Table S2).

References

1. T. Li, Z. Wang, Y. Wang, C. Wu, Y. Liang, M. Xia, C. Yu, H. Yun, W. Wang, Y. Wang, J. Guo, H. Herrmann and T. Wang, Chemical characteristics of cloud water and the impacts on aerosol properties at a subtropical mountain site in Hong Kong SAR, *Atmospheric Chemistry and Physics*, 2020, **20**, 391-407.

2. S. A. Brockman, E. V. Roden and A. D. Hegeman, Van Krevelen diagram visualization of high resolution-mass spectrometry metabolomics data with OpenVanKrevelen, *Metabolomics*, 2018, **14**, 1-5.

3. B. F. Mann, H. Chen, E. M. Herndon, R. K. Chu, N. Tolic, E. F. Portier, T. Roy Chowdhury, E. W. Robinson, S. J. Callister and S. D. Wullschleger, Indexing permafrost soil organic matter degradation using high-resolution mass spectrometry, *PLoS One*, 2015, **10**, e0130557.

4. A. Bianco, L. Deguillaume, M. Vaïtilingom, E. Nicol, J.-L. Baray, N. Chaumerliac and M. Bridoux, Molecular characterization of cloud water samples collected at the puy de Dôme (France) by Fourier Transform Ion Cyclotron Resonance Mass Spectrometry, *Environmental science & technology*, 2018, **52**, 10275-10285.

5. C. Zhang, B. Li, R. Jadeja and Y. C. Hung, Effects of Electrolyzed Oxidizing Water on Inactivation of Bacillus subtilis and Bacillus cereus Spores in Suspension and on Carriers, *J Food Sci*, 2016, **81**, M144-149.

6. A. Sündermann, L. F. Eggers and D. Schwudke, in *Encyclopedia of Lipidomics*, 2016, DOI: 10.1007/978-94-007-7864-1_88-1, ch. Chapter 88-1, pp. 1-4.

7. R. Helmus, T. L. Ter Laak, A. P. van Wezel, P. de Voogt and E. L. Schymanski, patRoon: open source software platform for environmental mass spectrometry based non-target screening, *Journal of Cheminformatics*, 2021, **13**, 1-25.

8. M. Meringer, S. Reinker, J. Zhang and A. Muller, MS/MS data improves automated determination of molecular formulas by mass spectrometry, *MATCH Commun. Math. Comput. Chem*, 2011, **65**, 259-290.

9. E. B. Kujawinski and M. D. Behn, Automated analysis of electrospray ionization Fourier transform ion cyclotron resonance mass spectra of natural organic matter, *Analytical chemistry*, 2006, **78**, 4363-4373.

10. B. P. Koch and T. Dittmar, From mass to structure: An aromaticity index for high-resolution mass data of natural organic matter, *Rapid communications in mass spectrometry*, 2006, **20**, 926-932.

11. D. M. McKnight, E. W. Boyer, P. K. Westerhoff, P. T. Doran, T. Kulbe and D. T.

Andersen, Spectrofluorometric characterization of dissolved organic matter for indication of precursor organic material and aromaticity, *Limnology and Oceanography*, 2001, **46**, 38-48.

12. M. Pucher, U. Wünsch, G. Weigelhofer, K. Murphy, T. Hein and D. Graeber, staRdom: versatile software for analyzing spectroscopic data of dissolved organic matter in R, *Water*, 2019, **11**, 2366.

13. S. Yue, L. Ren, T. Song, L. Li, Q. Xie, W. Li, M. Kang, W. Zhao, L. Wei and H. Ren, Abundance and diurnal trends of fluorescent bioaerosols in the troposphere over Mt. Tai, China, in spring, *Journal of Geophysical Research: Atmospheres*, 2019, **124**, 4158-4173.

14. Q. Chen, Y. Miyazaki, K. Kawamura, K. Matsumoto, S. Coburn, R. Volkamer, Y. Iwamoto, S. Kagami, Y. Deng and S. Ogawa, Characterization of chromophoric water-soluble organic matter in urban, forest, and marine aerosols by HR-ToF-AMS analysis and excitation–emission matrix spectroscopy, *Environmental Science & Technology*, 2016, **50**, 10351-10360.

15. C. Pöhlker, J. Huffman and U. Pöschl, Autofluorescence of atmospheric bioaerosols–fluorescent biomolecules and potential interferences, *Atmospheric Measurement Techniques*, 2012, **5**, 37-71.

16. G. Wu, P. Fu, K. Ram, J. Song, Q. Chen, K. Kawamura, X. Wan, S. Kang, X. Wang, A. Laskin and Z. Cong, Fluorescence characteristics of water-soluble organic carbon in atmospheric aerosol☆, *Environmental Pollution*, 2021, **268**, 115906.